Published in final edited form as:
Cell. 2013 July 18; 154(2): 391–402. doi:10.1016/j.cell.2013.06.010.

Cortical dynein and asymmetric membrane elongation coordinately position the spindle in anaphase

Tomomi Kiyomitsu[1,*] and **Iain M. Cheeseman**[1,*]

[1] Whitehead Institute for Biomedical Research, and Department of Biology, MIT Nine Cambridge Center Cambridge, MA 02142

SUMMARY

Mitotic spindle position defines the cell cleavage site during cytokinesis. However, the mechanisms that control spindle positioning to generate equal-sized daughter cells remain poorly understood. Here, we demonstrate that two mechanisms act coordinately to center the spindle during anaphase in symmetrically dividing human cells. First, the spindle is positioned directly by the microtubule-based motor dynein, which we demonstrate is targeted to the cell cortex by two distinct pathways: a Gαi/LGN/NuMA-dependent pathway, and a 4.1G/R and NuMA-dependent anaphase-specific pathway. Second, we find that asymmetric plasma membrane elongation occurs in response to spindle mis-positioning to alter the cellular boundaries relative to the spindle. Asymmetric membrane elongation is promoted by chromosome-derived Ran-GTP signals that locally reduce Anillin at the growing cell cortex. In asymmetrically elongating cells, dynein-dependent spindle anchoring at the stationary cell cortex ensures proper spindle positioning. Our results reveal the anaphase-specific spindle centering systems that achieve equal-sized cell division.

Keywords

spindle positioning; dynein; mitosis; cell division

INTRODUCTION

Cell division is a fundamental process required to increase cell number and alter cell types. During the development of multicellular organisms, cells undergo both symmetric and asymmetric cell divisions (Horvitz and Herskowitz, 1992; Morin and Bellaiche, 2011). Symmetric cell division generates identical daughter cells for clonal expansion, whereas asymmetric cell division creates distinct daughter cells to increase cell type diversity. Symmetric and asymmetric cell divisions can vary in the distribution of cell fate factors (Knoblich, 2008), and also in the size of the resulting daughter cells with a subset of asymmetric divisions generating cells of differing sizes (Gonczy, 2008; Siller and Doe, 2009). To specify these different cell division types, a key requirement is to orient and position the mitotic spindle within the cell. Spindle position dictates the site at which the cytokinetic cleavage furrow is formed through signals emanating from the spindle midzone

* Corresponding authors: Phone: (617) 324-2503 Fax: (617) 258-5578 tomomi.kiyomitsu@gmail.com, icheese@wi.mit.edu.

and astral microtubules during anaphase (Burgess and Chang, 2005). To achieve a symmetric cell division with two equal-sized daughter cells, the mitotic spindle must be precisely positioned in the center of the dividing cell.

The position of the mitotic spindle is controlled, at least in part, by dynein-dependent cortical pulling forces exerted on astral microtubules (Gonczy, 2008). Dynein consists of a catalytic heavy chain (DHC) and non-catalytic subunits that interact with additional binding partners including the dynactin complex to control the localization and function of the dynein motor (Kardon and Vale, 2009). We and others have previously demonstrated that dynein and dynactin are recruited to the cell cortex by the Gαi-LGN-NuMA complex in symmetrically dividing human cells to generate pulling forces that control spindle position and orientation during metaphase (Kiyomitsu and Cheeseman, 2012; Kotak et al., 2012; Woodard et al., 2010). However, although the loss of LGN randomizes spindle orientation, it does not result in unequal-sized daughter cells (Kiyomitsu and Cheeseman, 2012). This indicates that additional mechanisms must act to center the spindle and generate equivalently-sized daughter cells.

Here, we analyzed the mechanisms that position the spindle within the cell during anaphase. We find that two parallel pathways involving LGN and 4.1 family proteins target dynein to the cell cortex to ensure equal-sized cell division. Unexpectedly, we find that cells also control spindle position by asymmetrically elongating their plasma membrane during anaphase to adjust the cellular boundaries and center the spindle within the cell. Thus, to achieve a symmetric cell division, cells coordinately control the movement of the spindle and the position of the cell boundaries to define a central cell cleavage site.

RESULTS

NuMA and dynein are recruited to the anaphase cell cortex independently of LGN and Gαi

LGN depletion eliminates dynein heavy chain (DHC-GFP) localization to the cell cortex during metaphase and randomizes spindle orientation (Fig.1A; Kiyomitsu and Cheeseman, 2012). However, most LGN-depleted cells ultimately generate equal-sized daughter cells (Fig. 1A; see below), suggesting that additional mechanisms act to specify the cell cleavage site in the absence of LGN. Indeed, we found that dynein was recruited to the cell cortex during anaphase in 95% of LGN depleted cells (Fig. 1A). To dissect the requirements for cortical dynein recruitment during anaphase, we analyzed the localization of dynein, dynactin, and NuMA following the depletion of LGN, Gαi, or NuMA by RNAi in HeLa cells. Depletion of LGN or Gαi eliminated the cortical localization of dynein (DHC-GFP), the dynactin subunit p150, and NuMA during metaphase (Fig. S1A; Kiyomitsu and Cheeseman, 2012), but not anaphase (Fig. 1B, C, S1B). In contrast, NuMA depletion reduced the localization of dynein/dynactin to both the metaphase and anaphase cell cortex (Fig. 1B, D and S1B, C). We note that the residual NuMA remaining following these depletion conditions (Fig. 1D) is likely sufficient to suppress the previously defined contribution of NuMA to mitotic spindle assembly (Merdes et al., 1996).

As we found that NuMA was required for cortical dynein recruitment during anaphase, we next analyzed NuMA localization. NuMA and dynein/dynactin displayed increased levels at

the cell cortex during anaphase relative to metaphase (Fig. 1E, S1D, E; Collins et al., 2012), whereas Gαi1 and LGN did not (Fig. 1E, S1E). This suggests that an additional pool of NuMA and dynein is recruited to the cell cortex at anaphase onset. Consistent with two populations of NuMA, we found that the C-terminal globular region of NuMA (NuMA-C) localized only to the cell cortex during anaphase, but not metaphase (Fig. 1F, S1F-H). LGN depletion did not affect the localization of NuMA-C to the anaphase cell cortex (Fig. S1I). Inhibition of cyclin-dependent kinase (CDK) activity using Flavopiridol (Fla) in cells treated with the microtubule depolymerizing drug nocodazole caused NuMA-C to accumulate at the cell cortex (Fig. 1G), suggesting that this localization is negatively regulated by CDK. The C-terminal region of NuMA contains multiple CDK consensus phosphorylation sites and a phospho-deficient mutant of full length NuMA (“3A”; T2015A T2055A S2087A) shows increased accumulation at the cell cortex during metaphase (Compton and Luo, 1995). Consistent with a role for these phosphorylation sites in regulating cortical recruitment, we found that GFP-NuMA-C 3A localized prematurely to the cell cortex during metaphase (Fig. 1F, bottom). Taken together, these results suggest that the NuMA C-terminal region promotes the LGN-independent targeting of NuMA to the cell cortex during anaphase and is regulated by CDK-dependent phosphorylation.

Band 4.1 proteins are required for the anaphase-specific cortical localization of NuMA and dynein

We hypothesized that NuMA-C 3A localizes to the metaphase cell cortex by interacting with cortical receptors that normally bind to dephosphorylated NuMA during anaphase. To identify the cellular binding partners for NuMA-C 3A, we isolated GFP-NuMA-C 3A from HeLa cells arrested in mitosis using nocodazole. Mass spectrometry analysis indicated that GFP-NuMA-C 3A co-purified with 4.1G (also known as band 4.1-like 2 protein/ EPB41L2) and 4.1R (also known as band 4.1 protein/ EPB41) (Fig. 2A), but not with LGN. Similar purifications using an internally truncated version of NuMA lacking a large portion of the coiled-coil ($NuMA^{Bonsai}$; Fig. S1F, G) also isolated 4.1G (Fig. 2A). GFP tagged 4.1G and 4.1R localize to the cell cortex throughout mitosis (Fig. 2B), similar to endogenous 4.1G (Fig. S2A). In reciprocal purifications, we found that GFP-4.1G isolated NuMA, but not LGN (Fig. 2A). In our previous GFP-LGN purifications, we isolated NuMA, Gαi, dynein, and dynactin, but not 4.1 proteins (Kiyomitsu and Cheeseman, 2012). Previous 2-hybrid studies identified an interaction between NuMA and 4.1 proteins (Mattagajasingh et al., 1999; Ye et al., 1999), but did not test the relationship between these proteins at the cell cortex. Importantly, co-depletion of 4.1G and 4.1R, but not LGN depletion, disrupted the cortical localization of GFP-NuMA-C 3A during metaphase (Fig. 2C, S2B). These results suggest that band 4.1 proteins associate with the NuMA C-terminus to target it to the cell cortex.

Based on the results described above, we hypothesized that there are two parallel pathways for cortical NuMA/dynein/dynactin recruitment in HeLa cells: an LGN-dependent pathway and a 4.1-dependent anaphase-specific pathway. To test this, we depleted LGN and 4.1 either individually or in combination by RNAi (Fig. 2D, S2C). Individual depletion of LGN abolished cortical NuMA and dynein/dynactin localization during metaphase, but not anaphase (Fig. 2D, E, and S1A), whereas 4.1G/R depletion did not affect cortical NuMA or

dynein/dynactin localization during either metaphase or anaphase (Fig. 2D, E, S1A, S2D). In contrast, co-depletion of LGN and 4.1G/R abolished the cortical localization of NuMA, dynein, and dynactin during both metaphase and anaphase (Fig. 2D, E, S1A, S2D). In LGN and 4.1G/R co-depleted cells, expression of RNAi-resistant versions of either mCherry-LGN or mCherry-4.1G restored dynein localization to the cell cortex (Fig. 2F, S2E, F). Together, this suggests that an LGN-dependent pathway targets NuMA and dynein to the cell cortex during metaphase and maintains cortical dynein throughout anaphase and that a 4.1-dependent pathway recruits a second pool of NuMA and dynein in parallel to the LGN-dependent pathway during anaphase.

Artificial membrane targeting of the 4.1G C-terminal domain rescues cortical dynein localization in LGN and 4.1G/R co-depleted cells

We next sought to define the requirements for the ability of LGN and 4.1 to target NuMA and dynein to the cell cortex. In contrast to replacement with full length LGN, a LGN-C fragment lacking the NuMA binding N-terminal region localized to the plasma membrane, but failed to restore cortical dynein localization in LGN and 4.1G/R co-depleted cells (Fig. 2F, S2E). Similarly, expression of mCherry-4.1GΔCTD lacking a ~120 amino acid putative NuMA binding C-terminal domain (CTD) (Fig. 2G, S2G; Mattagajasingh et al., 1999; Ye et al., 1999), localized to the plasma membrane (Fig. 2G, S2H), but failed to restore cortical dynein localization in LGN and 4.1G/R co-depleted cells (Fig. 2F, G, S2F). Although the 4.1G-CTD itself does not localize to the membrane (Fig. S2H), artificial targeting of the 4.1G-CTD to the membrane using a membrane-targeting signal (N-terminus of neuromodulin; Mem-mCherry-4.1G-CTD) restored cortical dynein and NuMA localization during anaphase in LGN and 4.1G/R depleted cells (Fig. 2F, H, S2I, J). These results indicate that 4.1 proteins recruit NuMA and dynein to the anaphase cell cortex through their conserved C-terminal domain (CTD) (Fig. 2I).

LGN and 4.1G/R co-depletion results in unequal-sized cell division

Cortical dynein is thought to define daughter cell size by controlling spindle position during anaphase (Gonczy, 2008). However, it has not been possible to analyze the specific roles of cortical dynein in vertebrate cells as both dynein and NuMA play multiple roles in spindle structure, organization, and mitotic progression (Merdes et al., 1996). Co-depletion of LGN and 4.1G/R disrupted the localization of dynein to the cell cortex without affecting spindle structure, providing an ideal tool to test the contribution of cortical dynein to spindle positioning. HeLa cells normally divide to generate daughter cells of equivalent sizes (Fig. 3A, left). In contrast, co-depletion of LGN and 4.1G/R resulted in unequal-sized daughter cells for a subset of cell divisions (Fig. 3A, right). To quantify such unequal-sized cell divisions, we measured the ratio (R) of the areas of the two daughter cells (L – large; S – small) in control cells, LGN or 4.1G/R individually depleted cells, or LGN and 4.1G/R co-depleted cells (Fig. 3B). We found that R had an average value of 1.1 in control cells (Fig. 3B, S3A), corresponding to equivalently sized daughter cells. In LGN or 4.1G/R individual depletions, daughter cell size was subtly affected (Fig. 3B, C, S3A). In contrast, LGN and 4.1G/R co-depleted cells displayed highly unequal-sized cell divisions with 11.9% of cell divisions having an $R > 1.5$, a value never observed in control cells (Fig. 3A-C, S3A). In these unequal-sized daughters, the amount of DNA in each cell as visualized by mCherry-

histone H2B fluorescence was similar (Fig. 3A), indicating that sister chromosome segregation was not affected. Importantly, this unequal-sized cell division in the LGN and 4.1 co-depleted cells was rescued by artificial targeting of the 4.1G-CTD to the membrane (Fig. 3B, C, S3A, B), or by expression of siRNA-resistant full length 4.1G or LGN, but not 4.1GΔCTD (Fig. S3C, D). These results suggest that cortical dynein is critical for equal-sized cell division in symmetrically dividing human cells.

To analyze the effects of the unequal-sized cell divisions, we followed the behavior of the "larger" and "smaller" daughter cells in synchronized cultures (Fig. 3D). Larger daughter cells (labeled as L) always entered the next mitosis earlier (average duration = 24.5 hrs) than smaller cells (S, n = 13) and also earlier than normal "medium"-sized daughters (M; average duration = 30.8 hrs) resulting from a typical equal-sized cell division (Fig. 3E). Larger cell size may reduce the G1 phase for cell growth in HeLa cells and result in earlier entry into the next mitosis, similar to what is observed in yeast (Jorgensen and Tyers, 2004). All smaller sized cells showed a cell cycle delay and 15% of smaller cells underwent an apoptotic-like cell death during the period observed (Fig. 3D), suggesting that vertebrate cells may have a minimal cell size threshold for survival. These results suggest that cortical dynein functions during anaphase to ensure equal-sized cell division, and that the failure to generate proper cell size symmetry alters cell cycle progression in daughter cells.

Dynein-dependent spindle movement drives spindle centering during early anaphase

To visualize the spindle centering processes, we next monitored dynein (DHC-GFP), chromosomes (mCherry-H2B), and the cell cortex (Lifeact-mCherry) (Fig. 4A, D, E) during anaphase. For this analysis, we classified anaphase into two phases: early anaphase (~0-5 min post-anaphase onset, during which cell shape does not change), and late anaphase (~5-15 min post-anaphase onset, during which cells elongate their boundaries) (Fig. 4B). We found that 42% of control cells (which we term "Type I") entered anaphase with the spindle centrally positioned (Fig. 4A, B, D). For these cells, the distance between the cell center and the center of the separating sister chromatid masses (termed "Δ"; see Fig. S4A) was less than 1.65 μm at anaphase onset (red line in Fig. 4C) indicative of a central spindle position. This distance decreased further during early anaphase (blue line in Fig. 4C) such that the spindle was precisely centered prior to cell elongation during late anaphase. In contrast, 31% of control cells (which we term "Type II"), entered anaphase with the spindle mis-positioned (Δ > 1.65 μm), but subsequently corrected this positioning during early anaphase (Fig. 4B, C) by the movement of the spindle towards distal cell cortex (Fig. 4A, see kymograph). In these cells, dynein localized asymmetrically to the cell cortex at anaphase onset (Fig. 4A, right t = 0, arrow), which we have shown previously drives spindle movement during metaphase (Kiyomitsu and Cheeseman, 2012). Thus, the majority of control cells precisely positioned the spindle at the cell center by the end of early anaphase (Fig. 4B, C). This central spindle position was maintained during late anaphase during which the plasma membrane elongated near both spindle poles to increase the cellular boundaries and accommodate spindle elongation (Fig. 4D, top; Fig. 4E left, Movie S1).

We next sought to assess the role of cortical dynein in spindle centering during early anaphase. In LGN and 4.1G/R depleted cells, a subset of cells entered anaphase with a

central spindle position (Fig. 4B, Type I; Fig. 4D, bottom). Although these cells lack cortical dynein, the size of the mitotic spindle (~14 μm) relative to the diameter of a HeLa cell (~23 μm) could allow these cells to randomly "center" their spindle. Importantly, in LGN and 4.1G/R depleted cells, we almost never observed spindle movements that corrected spindle positioning during early anaphase (Fig. 4B, Type II). Together, although 74% of control cells center their spindle by the end of early anaphase, only 43% of LGN and 4.1G/R co-depleted cells display spindle centering at this time point (Fig. 4B). Even in cases where the spindle was centrally positioned, we found that sister chromatid separation and spindle elongation was strongly impaired in LGN and 4.1G/R co-depleted cells (Fig. 4D, E, S4C, D, Movie S2, S3). These results suggest that dynein-based cortical pulling forces contribute to both spindle centering and spindle elongation during anaphase.

Asymmetric plasma membrane elongation contributes to spindle positioning during late anaphase

The majority of control cells achieve a central spindle position during early anaphase (Fig. 4B). However, 25% of control cells (which we term "Type III") still have spindle-positioning defects at the end of early anaphase (Fig. 4C, S4B). To determine the mechanisms by which this spindle mis-position is corrected, we visualized spindle positioning, spindle elongation, and cell shape reorganization. Unexpectedly, we found that in cells with an off-centered spindle during late anaphase, the plasma membrane elongated asymmetrically such that only one side of the polar membrane region elongated, with the other side remaining stationary (Fig. 5A bottom, 5B right, Movie S4). This asymmetric membrane elongation is different from the symmetric anaphase membrane elongation that occurs in Type I and II cells (Fig. 4B, D, E) in which both sides of the polar membrane elongate equally during anaphase (Fig. 5A top, 5B left, Movie S5). To our knowledge, such an asymmetric membrane elongation behavior during mitosis in symmetrically dividing cells has not been reported previously. Asymmetric plasma membrane elongation is not the result of cell movement because the cells were stably attached to coverslips throughout mitosis (data not shown). In addition, asymmetric elongation is not due to a heterogeneous extrinsic cellular environment as we also observed this behavior in cells cultured on fibronectin coated L-pattern coverslips with similar frequencies (symmetric 56%, asymmetric 44%, n = 25, Fig. S5A). We also observed asymmetric membrane elongation during anaphase in non-transformed human Rpe1 cells (Fig. S5B).

Although the spindle also elongates coincident with this asymmetric membrane elongation, the polar membrane elongated faster than the spindle and increased the distance between the growing cell cortex and the nearest set of sister chromatids (Fig. 5C, bottom kymograph, S5C). Therefore, asymmetric membrane elongation had the net effect of correcting spindle position by altering the cellular boundaries relative to the mitotic spindle during anaphase (Fig. 4C, 5B). In summary, using a combination of directed spindle movements during early anaphase and asymmetric membrane elongation relative to the spindle during late anaphase, control cells ultimately positioned the spindle centrally resulting in an equal-sized cell division (Fig. 4B).

LGN and 4.1G/R co-depleted cells fail to anchor the mitotic spindle in asymmetrically elongating cells

Although LGN and 4.1G/R depleted cells showed defective spindle centering during early anaphase, these defects are not sufficient to explain the unequal-sized cell division observed in the depleted cells (Fig. 3A, B, 4D). Importantly, we found that more than 90% of the LGN and 4.1G/R co-depleted cells that divided unevenly (R > 1.5) displayed asymmetric membrane elongation (Fig. 5D, E, Movie S6). This suggests that asymmetric plasma membrane elongation results in unequal-sized cell division in the absence of cortical dynein. In control cells undergoing asymmetric membrane elongation, the distance between the stationary cell cortex and the nearest set of sister chromatids was constant during late anaphase (Fig. 5F, 5G, top). In these asymmetrically elongating cells, dynein localized to the stationary cell cortex (Fig. 5H, left, arrows) such that it could act to anchor the spindle and prevent its displacement. Indeed, based on the localization of the microtubule plus end tracking protein GFP-EB1, astral microtubules contact the stationary cell cortex during anaphase (Fig. S5D). In contrast, we found that in LGN and 4.1G/R co-depleted cells (Fig. 5H, right), asymmetric membrane elongation resulted in both sets of sister chromatids moving together towards the growing cell cortex (Fig. 5G, bottom). The distance between the stationary cell cortex and the nearest set of sister chromatids increased during late anaphase in LGN and 4.1G/R co-depleted cells (Fig. 5F, red). This pair-wise movement of sister chromatids resulted in an increased Δ with an average value of 1.97 μm (Fig. S4E) and displaced the spindle midzone and cell cleavage site resulting in unequal-sized daughter cells (Fig. 5D). These results suggest that cortical dynein prevents unequal-sized cell division in asymmetrically elongating cells in part by anchoring the spindle to the stationary cell cortex.

Membrane blebbing, but not exocytosis, contributes to asymmetric cortical expansion

We next analyzed the mechanisms of asymmetric plasma membrane elongation during anaphase. Expansion of the plasma membrane could occur by local secretion of new membrane from internal vesicles or remodeling of the existing plasma membrane as the cell flattens from its rounded mitotic state. To test whether secretion occurs at sites of polar membrane expansion, we visualized membranes by incubating cells with the membrane dye FM4-64. Internal vesicles were largely excluded from the growing polar cell cortex during asymmetric cell elongation in both HeLa and Rpe1 cells and instead enriched near the cytokinetic cleavage furrow (Fig. S6A-C). Therefore, asymmetric membrane elongation involves either remodeling of the pre-existing membrane or newly incorporated membranes deposited near the cleavage furrow, but not direct deposition of new membrane at the site of expansion.

We next analyzed plasma membrane remodeling events. During asymmetric membrane elongation in HeLa cells, we observed the presence of membrane blebs that formed only at the growing polar cell cortex (Fig. 6A, B, S6D). Based on the dynamic localization of GFP-Anillin, which provides a marker for retracting blebs (Charras et al., 2006), we found that the membrane blebs were sequentially formed throughout the growing cell cortex with rapid cycles (~60 sec) of initiation, expansion, and retraction (Fig. 6B, S6E, Movie S7). Bleb formation locally disrupted the cortical localization of LGN and 4.1G at the neck of the

blebs, although 4.1G, but not LGN, localized to the bleb membrane (Fig. S6F, G). Bleb formation disrupted pre-existing cortical actin structures at the neck of the bleb (Fig 6A, S6D; Charras and Paluch, 2008), but subsequently assembled new actin structures at the bleb membrane as visualized by Lifeact-mCherry (Fig. 6A t = 2, S6D). These cycles of bleb formation and contraction extended the cellular boundary and resulted in cortical expansion (Fig. 6A t=4, S6D, E), providing one potential mechanism to elongate the polar membrane. Treatment with low doses of the Rho kinase inhibitor Y27632 at concentrations that inhibit membrane blebbing without affecting cytokinesis (Sedzinski et al., 2011) partially reduced the frequency of asymmetric membrane elongation (Fig. S6H), suggesting that bleb formation contributes to asymmetric membrane expansion in HeLa cells. However, Rpe1 cells also undergo asymmetric membrane elongation, but do not display membrane blebbing (Fig. S5B), suggesting that additional mechanisms to promote membrane expansion also exist.

Chromosome-derived Ran-GTP signals reduce Anillin localization to the cell cortex and induce asymmetric membrane elongation

To define the basis for the asymmetric membrane elongation, we next analyzed the distance between the sister chromatids and the growing or stationary cell cortex at the start of membrane elongation (Fig. 6C). We found that increased proximity of chromosomes to the cell cortex strongly correlated with the asymmetric membrane elongation of the nearest cell cortex in both control and LGN and 4.1G/R co-depleted cells (Fig. 6A-C). This suggests that plasma membrane remodeling is sensitive to the proximity of the chromosomes on the spindle.

We hypothesized that the proximity of the chromosomes to the cell cortex may locally alter proteins that control cortical stiffness and contractility at the polar cell cortex resulting in membrane blebbing and other remodeling events. To test this, we analyzed the cortical proteins Anillin and myosin (D'Avino, 2009; Salbreux et al., 2012). In symmetrically elongating anaphase cells, GFP-Anillin and GFP-MRLC2 (myosin regulatory light chain) show reduced cortical localization to both polar regions (Fig. S6I). However, GFP-Anillin and GFP-MRLC2 were asymmetrically reduced at the growing cell cortex just prior to asymmetric membrane elongation (Fig. 6D; Fig. S6J), and appeared to depend upon the relative proximity of the mitotic spindle to the cell cortex. To test whether the local cortical reduction of these proteins is influenced by signals from the spindle poles, astral microtubules, or chromosomes, we treated cells with nocodazole to depolymerize microtubules. GFP-Anillin was locally reduced from the cell cortex in the vicinity of chromosome masses in nocodazole treated HeLa cells (Fig. 6E) and Rpe1 cells (Fig. S6K). GFP-MRLC2 was also reduced in the vicinity of chromosome masses, and this behavior was enhanced following CDK inhibition in both HeLa and Rpe1 cells (Fig. S6L). This local reduction of Anillin and myosin has the potential to contribute to membrane remodeling events including membrane blebbing. Indeed, we found that in addition to its established role in cytokinesis (Piekny and Glotzer, 2008), global Anillin depletion resulted in premature bleb formation during metaphase (Fig. 6F), which was never observed in control cells, and the formation of large membrane blebs during anaphase (Fig. 6G).

Previous work has shown that Ran regulates Anillin-mediated pseudocleavage formation in *Drosophila* syncytial embryos (Silverman-Gavrila et al., 2008). To analyze the contribution of chromosome-derived Ran-GTP signals in mammalian cells, we used tsBN2 cells, which contain a temperature sensitive mutation in RCC1 that prevents the formation of Ran-GTP at the restrictive temperature (Nishitani et al., 1991). In nocodazole treated tsBN2 cells, Anillin was reduced from the cell cortex in the vicinity of the chromosome masses at the permissive temperature (Fig. 7A, left) similar to HeLa cells (Fig. 6E). However, at the restrictive temperature, Anillin localized to the cell cortex even in the vicinity of chromosomes (Fig. 7A, right). The temperature shift did not affect cortical Anillin localization in the parental BHK cells that are wild type for RCC1 (data not shown). In contrast to disrupting Ran-GTP, treatment with inhibitors against Aurora B kinase, which forms a spatial gradient on metaphase chromosomes and the anaphase midzone (Fuller et al., 2008) did not strongly affect asymmetric Anillin localization (Fig. S7A). These results suggest that chromosome-derived Ran-GTP signals act to locally reduce Anillin from the cell cortex near chromosomes.

To test whether the proximity of chromosomes to the cell cortex is sufficient to cause asymmetric membrane elongation in the absence of the mitotic spindle during anaphase, we treated cells with nocodazole and induced mitotic exit by addition of the CDK inhibitor Flavopiridol. In cases where the chromosome mass was located at the center of the cell, membrane blebs and changes in plasma membrane organization were observed throughout the cell cortex (Fig. S7B; Niiya et al., 2005). In contrast, when the chromosome mass was located near the cell cortex, the plasma membrane underwent a dramatic asymmetric expansion in the vicinity of the chromosomes (Fig. 7B C, S7B, C, Movie S8) in the regions where Anillin, MRLC2, LGN, and dynein were locally excluded (Fig. 7B, S6L, S7C, D). As the chromosome-proximal cell cortex expanded, adjacent regions of the cell cortex contracted resulting in a “budding” event reminiscent of cytokinesis (Fig. 7B t=35, S7C, D). Although these asymmetric budding events result from artificial drug treatment, this process has similar features to the membrane reorganization events that normally occur during anaphase and cytokinesis (Petronczki et al., 2008), as it requires Plk1, Ect2, and Myosin II activity (Fig. S7E-G). We observed this asymmetric membrane elongation in both HeLa cells (Fig. 7B, S7C, D) and Rpe1 cells (Fig. S7H), with asymmetric membrane expansion correlating with the formation of membrane blebs in HeLa cells (Fig. 7B, S7C), but not Rpe1 cells similar to the unperturbed cells.

To test the contribution of Ran-GTP signals to this asymmetric membrane elongation, we analyzed membrane elongation in BHK and tsBN2 cells following nocodazole and Flavopiridol treatment. In BHK cells, the plasma membrane elongated in the vicinity of the chromosome mass (Fig. 7D). However, in tsBN2 cells at the restrictive temperature, the membrane did not elongate regardless of the proximity of the chromosome mass to the cell cortex (Fig. 7D). Taken together, these results suggest that when the spindle is displaced, chromosome-derived Ran-GTP signals locally reduce Anillin and other proteins from the polar cell cortex, which results in asymmetric membrane elongation to alter the cellular boundaries and correct spindle positioning during anaphase (Fig. 7F).

DISCUSSION

4.1G/R are anaphase-specific cortical receptors for NuMA and dynein

Here, we identified 4.1G and 4.1R as anaphase-specific cortical receptors for NuMA (Fig. 2A), which in turn recruits dynein/dynactin to the cell cortex (Fig. 2D). Our data suggest that CDK-dependent phosphorylation of the C-terminal region of NuMA at metaphase prevents NuMA from interacting with 4.1G/R (Fig. 1F, G) such that the 4.1G/R-NuMA pathway recruits dynein only during anaphase. 4.1 is a well-conserved multifunctional membrane protein (Diakowski et al., 2006), and 4.1R links the plasma membrane to spectrin-actin cytoskeleton in red blood cells (Bennett and Baines, 2001). We demonstrated that that highly conserved 4.1 C-terminal domain (CTD; Fig. S2G) is necessary and sufficient to recruit NuMA and dynein to the anaphase cell cortex (Fig. 2F-H, S2I). Although 4.1 and LGN display independent localization (Fig. S2E, F) suggesting that these two dynein recruitment pathways are functionally distinct, they may act synergistically to recruit cortical dynein during anaphase based on the observed defects in dynein localization when these pathways are depleted.

Both the LGN- and 4.1-dependent pathways for cortical dynein recruitment utilize NuMA as an adaptor molecule (Fig. 7E). Thus, cells could regulate both pathways simultaneously by controlling NuMA, such as through chromosome-derived Ran-GTP signals (Kiyomitsu and Cheeseman, 2012). In contrast, the presence of these dual pathways could allow cells to temporally and spatially control cortical pulling forces. For example, the 4.1-NuMA interaction, but not LGN-NuMA binding, is negatively regulated by CDK during metaphase, which may increase cortical pulling forces during anaphase to ensure proper spindle elongation. In addition, 4.1 proteins, but not LGN, localize to membrane blebs (Fig. S6F), which may facilitate rapid dynein recruitment to the newly formed cell cortex. There may also be additional temporal and spatial signals that act to control these different dynein recruitment pathways. For example, signals derived from central spindle may negatively regulate the interaction between NuMA and 4.1 at the equatorial cell cortex during anaphase (Fig. 2B, D, H). Differential regulation of these two pathways could also be used to generate asymmetric cortical pulling forces during development. We hypothesize that these LGN- and 4.1-dependent cortical dynein recruitment pathways will play important roles in tissues and multi-cellular organisms for both symmetric and asymmetric cell divisions. LGN, 4.1G, and 4.1R individual knockout mice are viable (Konno et al., 2008; Shi et al., 1999; Yang et al., 2011), although LGN knockout mice display randomized spindle orientation for the normally planar neuroepithelial divisions (Konno et al., 2008). In the future, it will be important to test the combined defects caused by simultaneously disrupting LGN and 4.1 proteins during development and in an intact organism.

Asymmetric plasma membrane elongation acts for spindle centering

In addition to dynein-dependent spindle movements, we found that spindle mis-positioning that persists into late anaphase can be corrected by asymmetric elongation of the polar plasma membrane. This asymmetric membrane elongation does not appear to be a result of the extrinsic cellular environment (Fig. S5A), but instead results from the mis-positioning of the anaphase spindle and separating sister chromatids within the cell (Fig. 6C). This

asymmetric cortical expansion can likely occur using several mechanisms, but does not appear to involve vesicle secretion at the polar cell membrane (Fig.S6A-C), and instead requires remodeling of the existing cell membrane. In some cell types, we found that membrane blebbing contributes to asymmetric membrane elongation in response to an off-centered position of the spindle and sister chromatids (Fig. 6A, B, S6H). Membrane blebbing at the polar cell cortex during cytokinesis has been proposed to stabilize cell shape by acting as a "release valve" for cortical contractility (Sedzinski et al., 2011). Our results reveal an additional function for membrane blebbing during cytokinesis to control spindle positioning such that sequential membrane blebbing disrupts the preexisting actin cell cortex and forms a new cell cortex to expand the cellular boundary (Fig. 6A, B, S6A, B). However, even in the absence of membrane blebbing, asymmetric expansion of the plasma membrane can occur through membrane remodelling (Fig. 7D, S5B, S7H).

During anaphase, we propose that a local reduction of cortical Anillin downstream of chromosome-derived Ran-GTP signals locally weakens the polar cell cortex and results in membrane expansion. Previous work has tested the existence of a chromosome-derived Ran-GTP gradient during metaphase (Kalab et al., 2006). A gradient of RanGTP also persists into early anaphase based on the use of established FRET sensors in HeLa cells (Petr Kalab, personal communication). However, additional signals from the spindle pole or astral microtubules may also affect the localization or activity of Anillin and other cortical proteins for cortical expansion. Anillin interacts with activated form of myosin to promote cortical contraction during cytokinesis (Straight et al., 2005). We propose that asymmetric localization of Anillin downstream of Ran-GTP also generates cortical myosin asymmetry during anaphase (Fig. 6D, S6J, L), which drives cortical contraction and relaxation at the stationary and growing cell cortex, respectively, for asymmetric membrane elongation (Fig. S6M). Importantly, in addition to the work shown here in equally dividing human cells, asymmetric cortical extension also occurs to generate unequal-sized daughter cells during asymmetric cell division in *C. elegans* and *Drosophila* neuroblasts (Connell et al., 2011; Ou et al., 2010). How cortical pulling forces and membrane elongation are differently regulated in symmetric and asymmetric cell divisions will be an exciting topic for future work. Finally, anaphase spindle elongation may also be critical for equal-sized cell division (Fig. 4D; Xiao et al., 2012) to generate a larger spindle structure that is more naturally placed in the middle of the dividing cell.

In conclusion, our results reveal that cortical dynein and membrane elongation coordinately control spindle positioning. Both mechanisms are autonomously regulated in response to spindle position and cooperatively center the spindle to achieve an equal-sized cell division.

Experimental Procedures

Cell culture and siRNA transfection

HeLa, Rpe1, BHK and tsBN2 cells were maintained as described previously (Kiyomitsu and Cheeseman, 2012). Clonal cell lines stably expressing GFP^{LAP} or mCherry fusions were generated as described previously (Schmidt et al., 2010). Plasmid DNA transfections were conducted using Effectene (QIAGEN). To inactivate RCC1, tsBN2 cells were cultured at 39.7°C for 2-3.5 hrs. To induce mitotic exit in the absence of microtubules, HeLa or Rpe1

cells were incubated for 3-6 hrs with 100 nM Nocodazole (Sigma Aldrich), and subsequently treated with 100 nM Nocodazole plus 5 μM Flavopiridol (Sigma Aldrich). Where indicated, cells were incubated with 16 μM FM4-64 (Molecular Probes), 10 μM Y27632 (EMD Biosciences), 10 μM BI2536 (Tocris), or 100 μM Blebbistatin (Sigma Aldrich).

RNAi experiments were conducted using the RNAi MAX transfection reagent (Invitrogen) in asynchronous cultures or combined with a double thymidine block to deplete proteins in synchronized cultures. For rescue experiments, plasmids were transfected 1 hr prior to siRNA transfection. For information regarding the siRNAs used, see the Supplemental Experimental Procedures.

Immunofluorescence and Microscopy

For live cell imaging, cells were cultured in CO_2 independent media (Invitrogen) with 50-100 ng/ml Hoechst33342 for 30 min prior to observation. Cells were fixed with 3% paraformaldehyde with 2% sucrose. Where indicated, cells were plated on L-patterned fibronectin coated coverslips (CYTOO). For information regarding antibodies used, see the Supplemental Experimental Procedures.

Images were acquired on a DeltaVision Core microscope (Applied Precision) equipped with a CoolSnap HQ2 CCD camera. For fixed cells, 30 Z-sections were acquired at 0.5-μm steps using an Olympus 40x, 1.35 NA U-PlanApo objective. For live cell imaging, 1-3 Z-sections were acquired at 1-2 μm steps with 1-5 min intervals. For Fig. 6B, a single focal image was obtained at 5 sec intervals. For the long term time-lapse imaging in Fig. 3D, images were acquired at 30 min intervals for 38 hrs. Images were deconvolved using the DeltaVision software. Equivalent exposure conditions and scaling was used as appropriate. Distance measurements were analyzed using Softworx (Applied Precision) and ImageJ/Fiji software. To measure the area ratio of daughter cells, Z-sections of bright field images were acquired at 1-μm steps to capture the entire cells during cytokinesis in living cells. Projected images were generated using Softworx (Applied Precision) and cell area was measured with ImageJ/Fiji software. Line scans for cortical fluorescence intensity and kymographs were generated using Metamorph (Molecular Devices) and Photoshop (Adobe), respectively. Movie files were generated using Softworx (Applied Precision) and GraphicConverter.

Affinity Purifications and Mass Spectrometry

GFP^{LAP} tagged NuMA-C 3A, $NuMA^{Bonsai}$, and 4.1G were isolated from HeLa cells as described previously (Kiyomitsu and Cheeseman, 2012). Purified proteins were identified by mass spectrometry using an LTQ XL Ion trap mass spectrometer (Thermo) using MudPIT and SEQUEST software.

Statistics

To determine the significance between the data obtained for two experimental conditions, a Student's T–test (GraphPad Software) or Z–test (McCallum Layton) was used as indicated in the figure legends.

Supplementary Material

Refer to Web version on PubMed Central for supplementary material.

Acknowledgments

We thank Defne Yarar, Adam Martin, Jonathan Coravos and members of the Cheeseman Lab for discussions and critical reading of the manuscript. We also thank Duane Compton for providing reagents. This work was supported by awards to IMC from the Leukemia & Lymphoma Society and the Human Frontiers Science Foundation, a grant from the NIH/National Institute of General Medical Sciences (GM088313), and a Research Scholar Grant (121776) from the American Cancer Society. IMC is a Thomas D. and Virginia W. Cabot Career Development Professor of Biology. TK is supported by a long-term fellowship of the Human Frontiers Science Program.

References

Bennett V, Baines AJ. Spectrin and ankyrin-based pathways: metazoan inventions for integrating cells into tissues. Physiological reviews. 2001; 81:1353–1392. [PubMed: 11427698]

Burgess DR, Chang F. Site selection for the cleavage furrow at cytokinesis. Trends Cell Biol. 2005; 15:156–162. [PubMed: 15752979]

Charras G, Paluch E. Blebs lead the way: how to migrate without lamellipodia. Nat Rev Mol Cell Biol. 2008; 9:730–736. [PubMed: 18628785]

Charras GT, Hu CK, Coughlin M, Mitchison TJ. Reassembly of contractile actin cortex in cell blebs. J Cell Biol. 2006; 175:477–490. [PubMed: 17088428]

Collins ES, Balchand SK, Faraci JL, Wadsworth P, Lee WL. Cell cycle-regulated cortical dynein/dynactin promotes symmetric cell division by differential pole motion in anaphase. Mol Biol Cell. 2012; 23:3380–3390. [PubMed: 22809624]

Compton DA, Luo C. Mutation of the predicted p34cdc2 phosphorylation sites in NuMA impair the assembly of the mitotic spindle and block mitosis. J Cell Sci. 1995; 108(Pt 2):621–633. [PubMed: 7769006]

Connell M, Cabernard C, Ricketson D, Doe CQ, Prehoda KE. Asymmetric cortical extension shifts cleavage furrow position in Drosophila neuroblasts. Mol Biol Cell. 2011; 22:4220–4226. [PubMed: 21937716]

D'Avino PP. How to scaffold the contractile ring for a safe cytokinesis - lessons from Anillin-related proteins. J Cell Sci. 2009; 122:1071–1079. [PubMed: 19339546]

Diakowski W, Grzybek M, Sikorski AF. Protein 4.1, a component of the erythrocyte membrane skeleton and its related homologue proteins forming the protein 4.1/FERM superfamily. Folia histochemica et cytobiologica / Polish Academy of Sciences, Polish Histochemical and Cytochemical Society. 2006; 44:231–248.

Fuller BG, Lampson MA, Foley EA, Rosasco-Nitcher S, Le KV, Tobelmann P, Brautigan DL, Stukenberg PT, Kapoor TM. Midzone activation of aurora B in anaphase produces an intracellular phosphorylation gradient. Nature. 2008; 453:1132–1136. [PubMed: 18463638]

Gonczy P. Mechanisms of asymmetric cell division: flies and worms pave the way. Nat Rev Mol Cell Biol. 2008; 9:355–366. [PubMed: 18431399]

Horvitz HR, Herskowitz I. Mechanisms of asymmetric cell division: two Bs or not two Bs, that is the question. Cell. 1992; 68:237–255. [PubMed: 1733500]

Jorgensen P, Tyers M. How cells coordinate growth and division. Curr Biol. 2004; 14:R1014–1027. [PubMed: 15589139]

Kalab P, Pralle A, Isacoff EY, Heald R, Weis K. Analysis of a RanGTP-regulated gradient in mitotic somatic cells. Nature. 2006; 440:697–701. [PubMed: 16572176]

Kardon JR, Vale RD. Regulators of the cytoplasmic dynein motor. Nat Rev Mol Cell Biol. 2009; 10:854–865. [PubMed: 19935668]

Kiyomitsu T, Cheeseman IM. Chromosome- and spindle-pole-derived signals generate an intrinsic code for spindle position and orientation. Nature cell biology. 2012; 14:311–317.

Knoblich JA. Mechanisms of asymmetric stem cell division. Cell. 2008; 132:583–597. [PubMed: 18295577]

Konno D, Shioi G, Shitamukai A, Mori A, Kiyonari H, Miyata T, Matsuzaki F. Neuroepithelial progenitors undergo LGN-dependent planar divisions to maintain self-renewability during mammalian neurogenesis. Nat Cell Biol. 2008; 10:93–101. [PubMed: 18084280]

Kotak S, Busso C, Gonczy P. Cortical dynein is critical for proper spindle positioning in human cells. J Cell Biol. 2012; 199:97–110. [PubMed: 23027904]

Mattagajasingh SN, Huang SC, Hartenstein JS, Snyder M, Marchesi VT, Benz EJ. A nonerythroid isoform of protein 4.1R interacts with the nuclear mitotic apparatus (NuMA) protein. J Cell Biol. 1999; 145:29–43. [PubMed: 10189366]

Merdes A, Ramyar K, Vechio JD, Cleveland DW. A complex of NuMA and cytoplasmic dynein is essential for mitotic spindle assembly. Cell. 1996; 87:447–458. [PubMed: 8898198]

Morin X, Bellaiche Y. Mitotic spindle orientation in asymmetric and symmetric cell divisions during animal development. Developmental cell. 2011; 21:102–119. [PubMed: 21763612]

Niiya F, Xie X, Lee KS, Inoue H, Miki T. Inhibition of cyclin-dependent kinase 1 induces cytokinesis without chromosome segregation in an ECT2 and MgcRacGAP-dependent manner. J Biol Chem. 2005; 280:36502–36509. [PubMed: 16118207]

Nishitani H, Ohtsubo M, Yamashita K, Iida H, Pines J, Yasudo H, Shibata Y, Hunter T, Nishimoto T. Loss of RCC1, a nuclear DNA-binding protein, uncouples the completion of DNA replication from the activation of cdc2 protein kinase and mitosis. Embo J. 1991; 10:1555–1564. [PubMed: 1851087]

Ou G, Stuurman N, D'Ambrosio M, Vale RD. Polarized myosin produces unequal-size daughters during asymmetric cell division. Science. 2010; 330:677–680. [PubMed: 20929735]

Petronczki M, Lenart P, Peters JM. Polo on the Rise-from Mitotic Entry to Cytokinesis with Plk1. Developmental cell. 2008; 14:646–659. [PubMed: 18477449]

Piekny AJ, Glotzer M. Anillin is a scaffold protein that links RhoA, actin, and myosin during cytokinesis. Curr Biol. 2008; 18:30–36. [PubMed: 18158243]

Salbreux G, Charras G, Paluch E. Actin cortex mechanics and cellular morphogenesis. Trends Cell Biol. 2012; 22:536–545. [PubMed: 22871642]

Schmidt JC, Kiyomitsu T, Hori T, Backer CB, Fukagawa T, Cheeseman IM. Aurora B kinase controls the targeting of the Astrin-SKAP complex to bioriented kinetochores. J Cell Biol. 2010; 191:269–280. [PubMed: 20937697]

Sedzinski J, Biro M, Oswald A, Tinevez JY, Salbreux G, Paluch E. Polar actomyosin contractility destabilizes the position of the cytokinetic furrow. Nature. 2011; 476:462–466. [PubMed: 21822289]

Shi ZT, Afzal V, Coller B, Patel D, Chasis JA, Parra M, Lee G, Paszty C, Stevens M, Walensky L, et al. Protein 4.1R-deficient mice are viable but have erythroid membrane skeleton abnormalities. The Journal of clinical investigation. 1999; 103:331–340. [PubMed: 9927493]

Siller KH, Doe CQ. Spindle orientation during asymmetric cell division. Nat Cell Biol. 2009; 11:365–374. [PubMed: 19337318]

Silverman-Gavrila RV, Hales KG, Wilde A. Anillin-mediated targeting of peanut to pseudocleavage furrows is regulated by the GTPase Ran. Mol Biol Cell. 2008; 19:3735–3744. [PubMed: 18579688]

Straight AF, Field CM, Mitchison TJ. Anillin binds nonmuscle myosin II and regulates the contractile ring. Mol Biol Cell. 2005; 16:193–201. [PubMed: 15496454]

Woodard GE, Huang NN, Cho H, Miki T, Tall GG, Kehrl JH. Ric-8A and Gi alpha recruit LGN, NuMA, and dynein to the cell cortex to help orient the mitotic spindle. Molecular and cellular biology. 2010; 30:3519–3530. [PubMed: 20479129]

Xiao Z, Wan Q, Du Q, Zheng Z. Galpha/LGN-mediated asymmetric spindle positioning does not lead to unequal cleavage of the mother cell in 3-D cultured MDCK cells. Biochem Biophys Res Commun. 2012; 420:888–894. [PubMed: 22469469]

Yang S, Weng H, Chen L, Guo X, Parra M, Conboy J, Debnath G, Lambert AJ, Peters LL, Baines AJ, et al. Lack of protein 4.1G causes altered expression and localization of the cell adhesion molecule

nectin-like 4 in testis and can cause male infertility. Molecular and cellular biology. 2011; 31:2276–2286. [PubMed: 21482674]

Ye K, Compton DA, Lai MM, Walensky LD, Snyder SH. Protein 4.1N binding to nuclear mitotic apparatus protein in PC12 cells mediates the antiproliferative actions of nerve growth factor. J Neurosci. 1999; 19:10747–10756. [PubMed: 10594058]

HIGHLIGHTS

- 4.1 family proteins are anaphase-specific cortical receptors for NuMA and dynein
- Cortical dynein is critical for spindle positioning and equal-sized cell division
- Centering can also occur by asymmetric membrane elongation relative to the spindle
- Chromosome-derived RanGTP signals control cortical proteins and membrane elongation

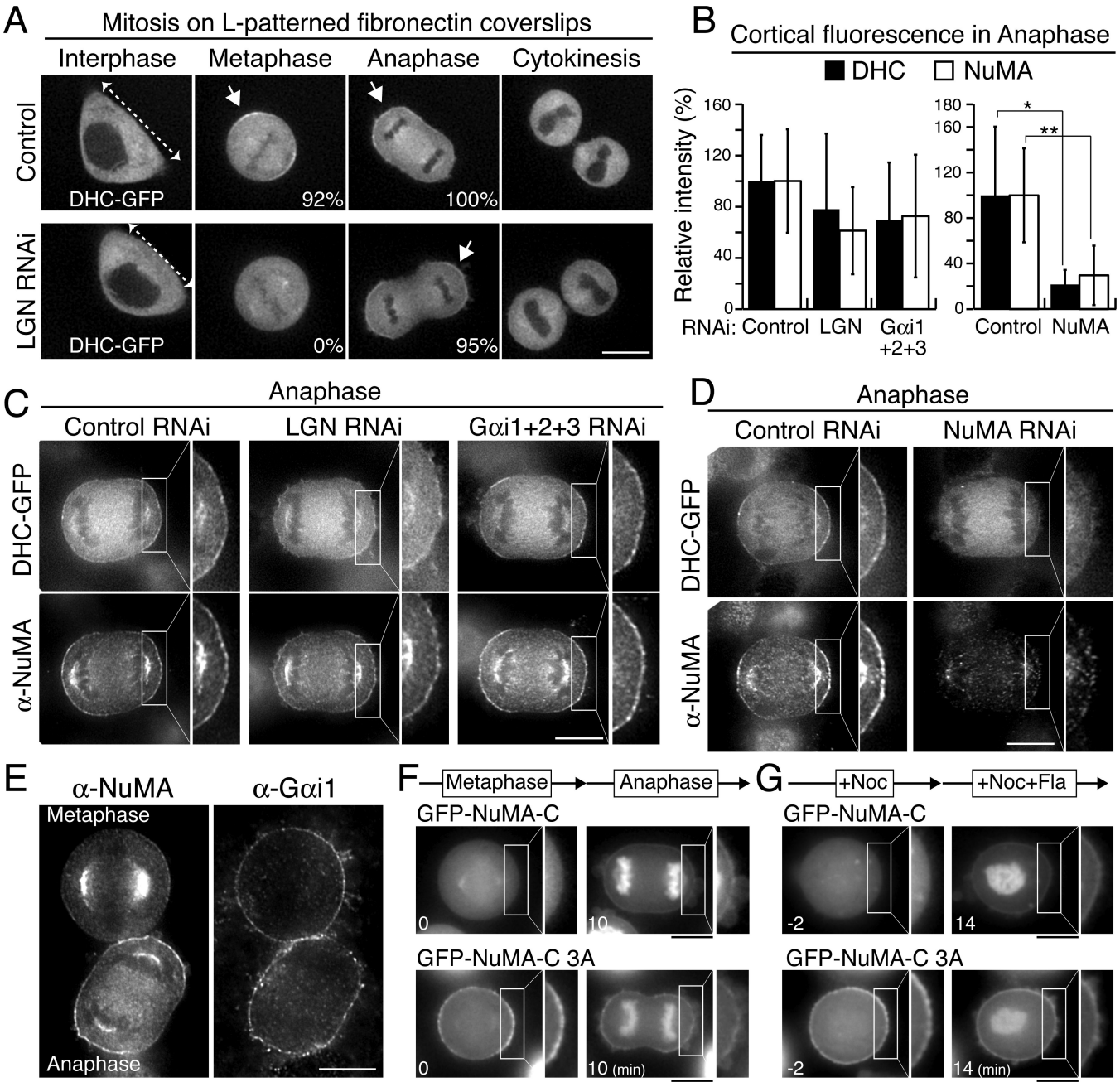

Figure 1. Dynein and NuMA are recruited to the cell cortex independently of Gαi and LGN during anaphase

(*A*) Fluorescent images of DHC-GFP from time-lapse movies of HeLa cells cultured on L-patterned fibronectin-coated coverslips. Control cells (top), but not LGN depleted cells (bottom), divide along the hypotenuse of the L (dashed arrows). Percentages indicate the frequency of cortical dynein localization (indicated by arrows) in controls (n=25 cells) and LGN depleted cells (n=21 cells) (*B*) Quantification of DHC-GFP and NuMA cortical fluorescence intensity in the indicated conditions (mean ± SD; n = 12-27 line scans from 4-9 cells). * indicates a statistically significant difference based on a student's T test (*p = 0.001, **p < 0.0001) (*C*, *D*) Immunofluorescence images of DHC-GFP and NuMA in control HeLa

cells and the indicated depletions. (*E*) Immunofluorescence images of NuMA and Gαi-1 in metaphase (top) and anaphase cells (bottom). (*F*) Fluorescent images of GFP-NuMA-C (top) and a GFP-NuMA-C 3A mutant (bottom) from time-lapse movies. (*G*) Time-lapse images of nocodazole (Noc) arrested cells expressing GFP-NuMA-C (top) or a GFP-NuMA-C 3A mutant (bottom). Nocodazole and Flavopiridol (Fla) were added at t=0 min. Scale bars, 10 μm. See also Figure S1.

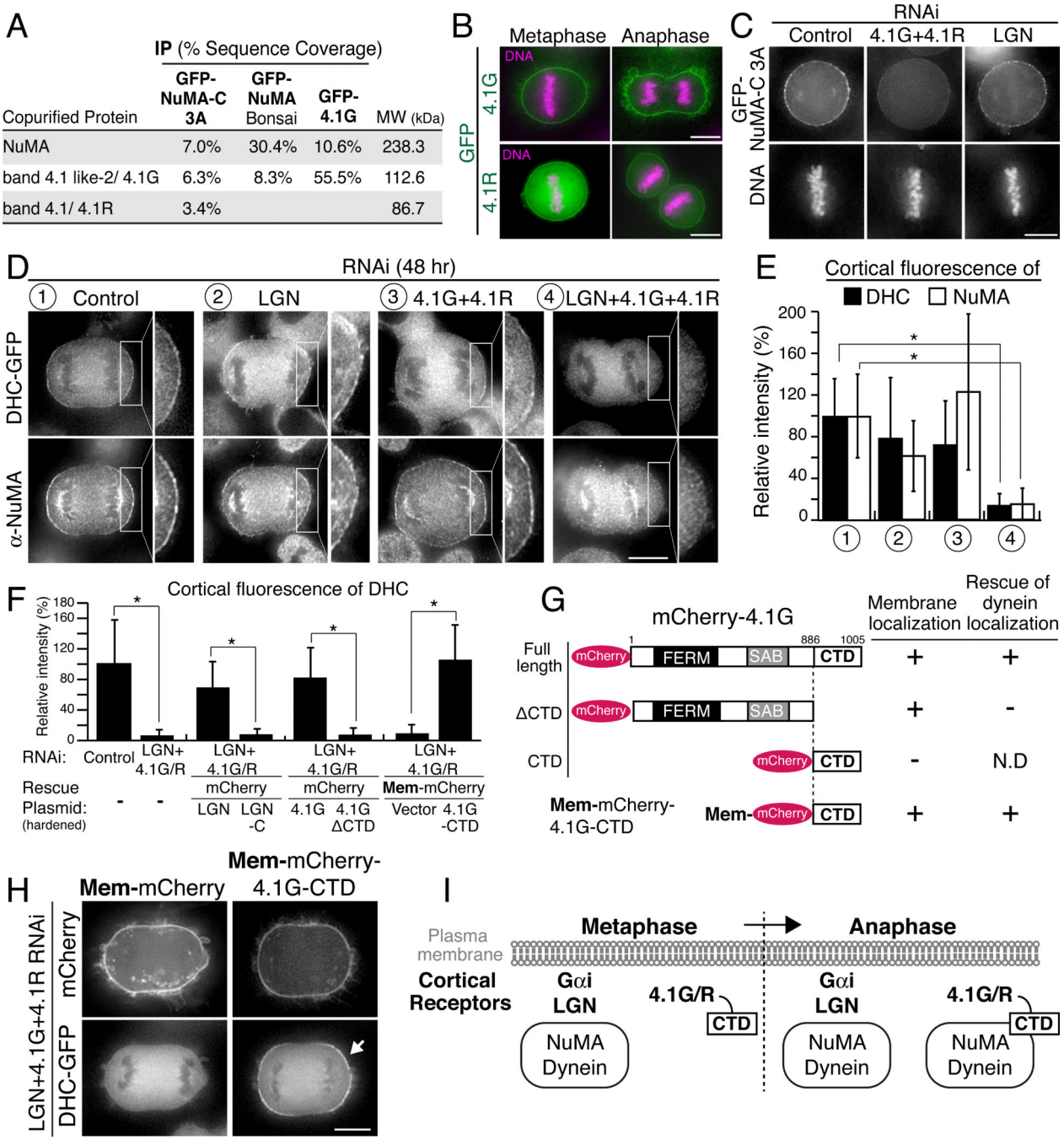

Figure 2. 4.1G and 4.1R are anaphase-specific cortical receptors for NuMA and dynein

(*A*) Data from the mass spectrometric analysis of the indicated affinity purifications listing the percentage sequence coverage. (*B*) Fluorescent images of HeLa cells expressing GFP-4.1G (isoform a, NP_001422) or GFP-4.1R (IMAGE clone 40001729). (*C*) Fluorescent images of GFP-NuMA-C 3A and DNA in control cells and the indicated RNAi-based depletions. (*D*) Immunofluorescence images of DHC-GFP and NuMA in control cells and the indicated depletions. (*E*) Quantification of DHC-GFP and NuMA cortical fluorescence intensity in the indicated conditions (mean ± SD; n = 12-36 line scans from 4-12 cells, * p <

0.0001) (*F*) Quantification of DHC-GFP cortical fluorescence intensity from the indicated conditions (mean ± SD; n = 27-30 line scans from 9-10 cells, * $p < 0.0001$) (*G*) Diagram showing full length 4.1G and the tested truncation fragments. The previously defined FERM, SAB and CTD domains (Diakowski et al., 2006) are indicated. Right, summary of membrane localization and rescue of cortical dynein localization by the indicated 4.1 fragments. (*H*) Fluorescence images showing rescue of DHC-GFP localization by membrane targeted 4.1G-CTD (arrow) in LGN and 4.1 co-depleted cells. (*I*) Diagram showing the cortical dynein receptors during metaphase and anaphase. Scale bars, 10 μm. See also Figure S2.

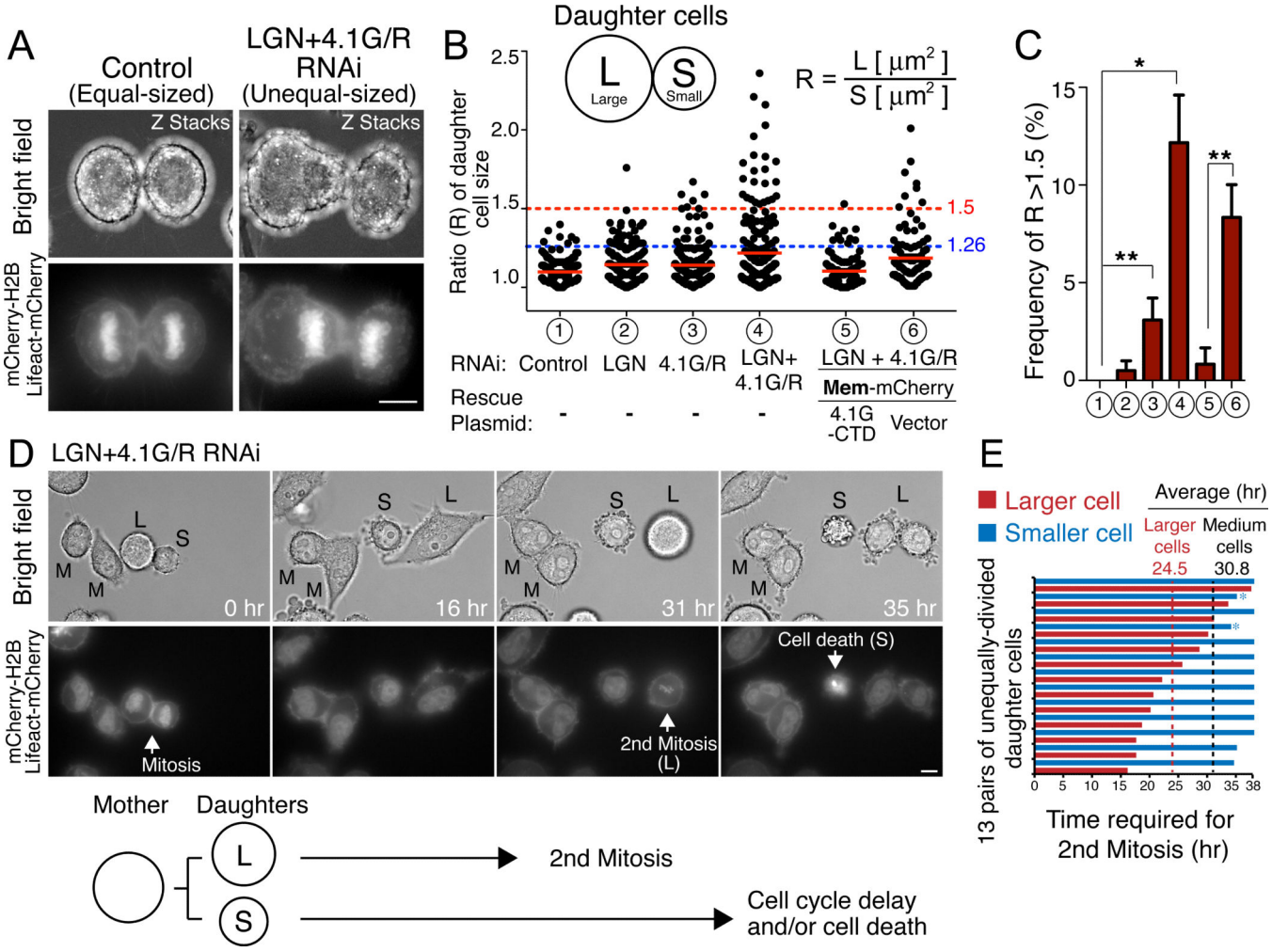

Figure 3. LGN and 4.1G/R co-depletion results in unequal-sized daughter cells

(*A*) Collapsed Z-stack images of bright field (top) and mCherry-H2B and Lifeact-mCherry (bottom) in control HeLa cells (left) and LGN+4.1G/R co-depleted cells (right). (*B*) Scatter plots of the relative area ratio (R) of daughter cells in the indicated depletions and rescue conditions. Red lines indicate means. (*C*) Quantification of the data from (B) showing the frequency of cells with R>1.5 in the indicated depletions ± SD. * indicates statistical difference from the control with either 99.9% (*) or 95%(**) confidence interval based on a *z*-test. (*D*) Top, time-lapse images of bright field (top) and mCherry-H2B and Lifeact-mCherry (bottom) in synchronized LGN and 4.1G/R co-depleted cells. L, M, and S indicate larger, medium and smaller cells, respectively. Bottom, diagram showing the phenotypes for larger and smaller daughter cells. (*E*) Graph showing the cell cycle duration required for the 2nd mitotic entry in larger (red) and smaller (blue) daughter cells. * indicates smaller cells showing apoptotic-like cell death. Dashed lines indicate the average duration in larger cells (red, n=13) and medium-sized cells (black, n=26). Scale bars, 10 μm. See also Figure S3.

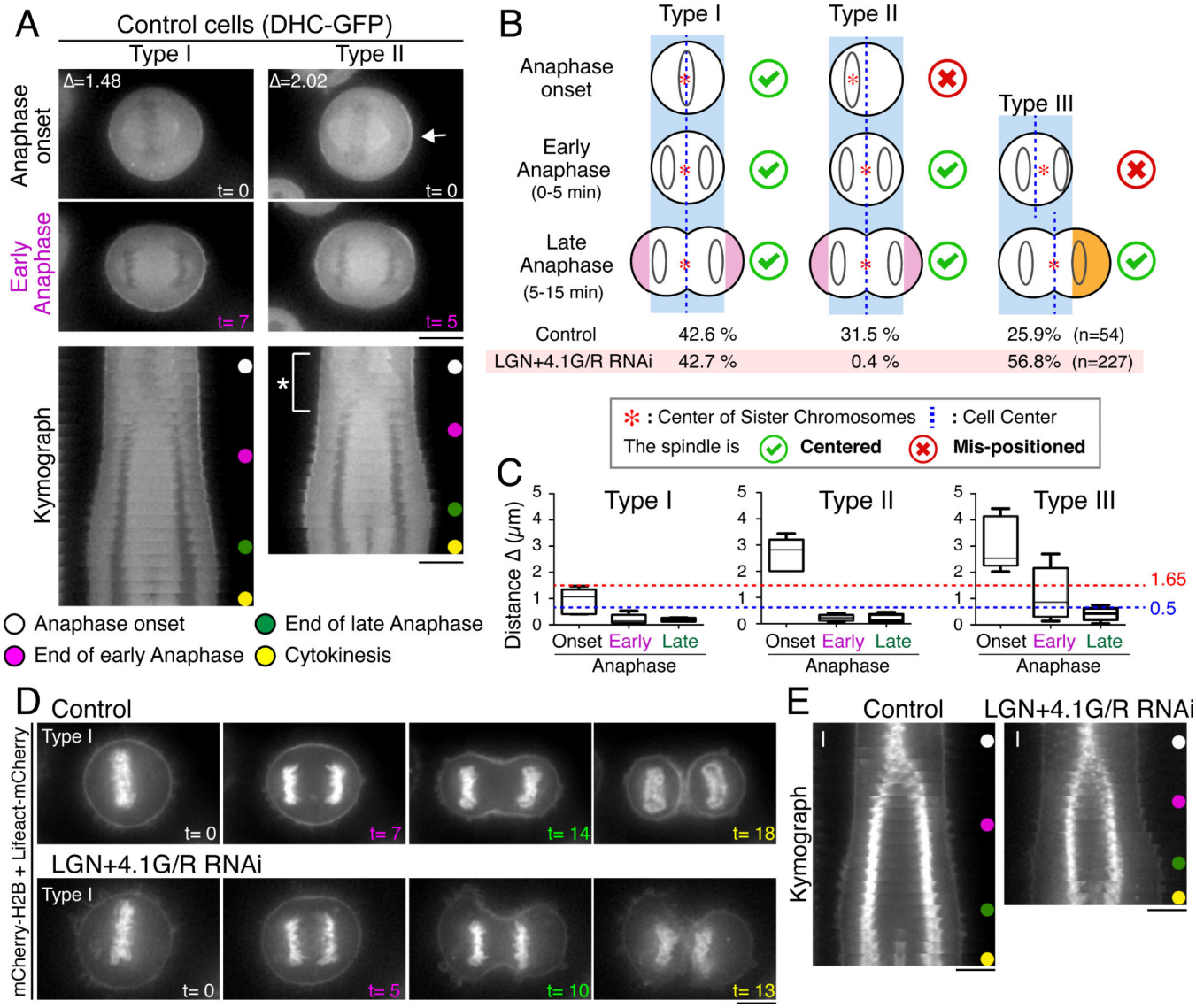

Figure 4. Dynein-dependent spindle movement drives spindle centering during early anaphase

(*A*) Top, time-lapse images showing DHC-GFP in a Type I (left) and Type II (right) cell. Bottom, kymographs showing the movements of dynein at 1 min intervals. Arrow indicates cortical dynein. * indicates spindle movement during early anaphase. (*B*) Diagram summarizing the 3 types of cell behavior for their anaphase spindle centering processes. Cells were classified based on the position of chromosomes at anaphase onset and the type of membrane elongation. The frequency of each class in control and LGN and 4.1G/R co-depleted cells is indicated. (*C*) Box plots of Δ (the distance between the cell center and the center of the sister chromatids) in control cells at anaphase onset, and the end of early and late anaphase. The red and blue dashed lines indicate Δ of 1.65, and 0.5, respectively (see Fig. S4A for details). n≥5 cells for each condition. (*D*) Time-lapse images of equally dividing Type I cells in control (top; Movie S1) and LGN and 4.1G/R co-depleted cells (bottom; Movie S2). (*E*) Kymographs generated from the image sequences in (D) showing

chromosome movements and the cell cortex at 1 min intervals. Scale bars, 10 μm. See also Figure S4.

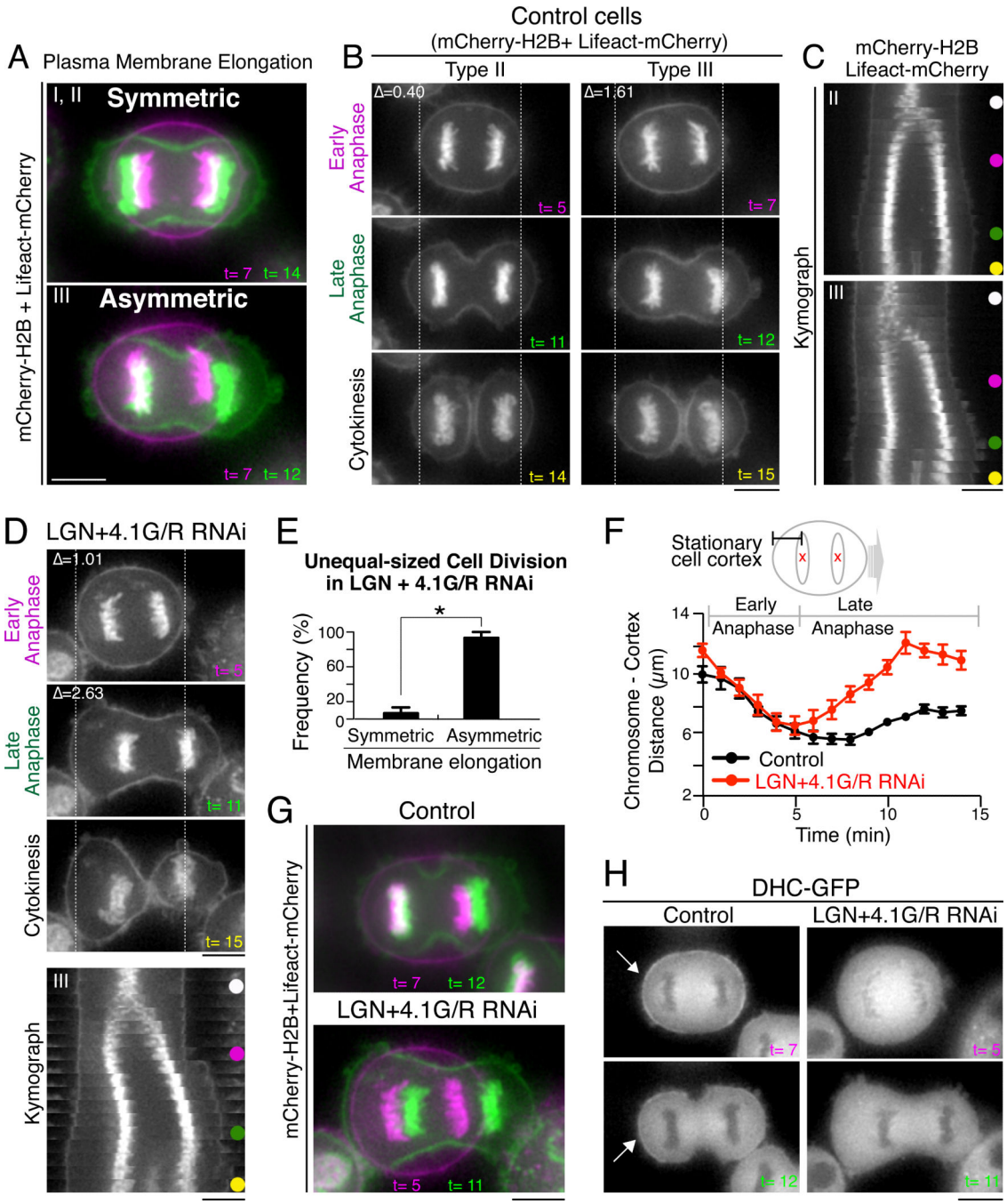

Figure 5. Asymmetric plasma membrane elongation and cortical dynein coordinately center the spindle during late anaphase

(*A*) Merged fluorescent images of symmetrically or asymmetrically elongating cells at the end of early anaphase (magenta) and late anaphase (green) (*B*) Time-lapse images in Type II and Type III cells (Movie S4, S5). Dashed lines indicate cellular boundaries at early anaphase. (*C*) Kymographs resulting from image sequences in (B) showing the movements of the chromosomes and the cell cortex at 1 min intervals. (*D*) Time-lapse images (top) and corresponding kymographs (bottom; 1 min intervals) showing mCherry-H2B and Lifeact-mCherry in unequally dividing Type III cells co-depleted for LGN and 4.1G/R (Movie S6).

Dashed lines indicate cellular boundaries at early anaphase. (*E*) Quantification of membrane elongation in unequally dividing (R>1.5) cells caused by LGN and 4.1G/R co-depletion (n=16). (*F*) Graph showing sister chromatid distance from the stationary cell cortex for control (black, n=5) and unequally dividing LGN and 4.1G/R co-depleted cells (red, n=5). All sequences were time-aligned with respect to anaphase onset (t=0). Error bars represent the S.E.M. (*G*) Merged images of cells at the end of early anaphase (magenta) and anaphase B (green) in asymmetrically elongating control (top) and LGN and 4.1G/R co-depleted cells (bottom). (*H*) Images showing DHC-GFP in asymmetrically elongating control (left) and LGN and 4.1G/R co-depleted cells corresponding to (G). Arrows indicate dynein localization to the stationary cell cortex. Scale bars, 10 μm. See also Figure S5.

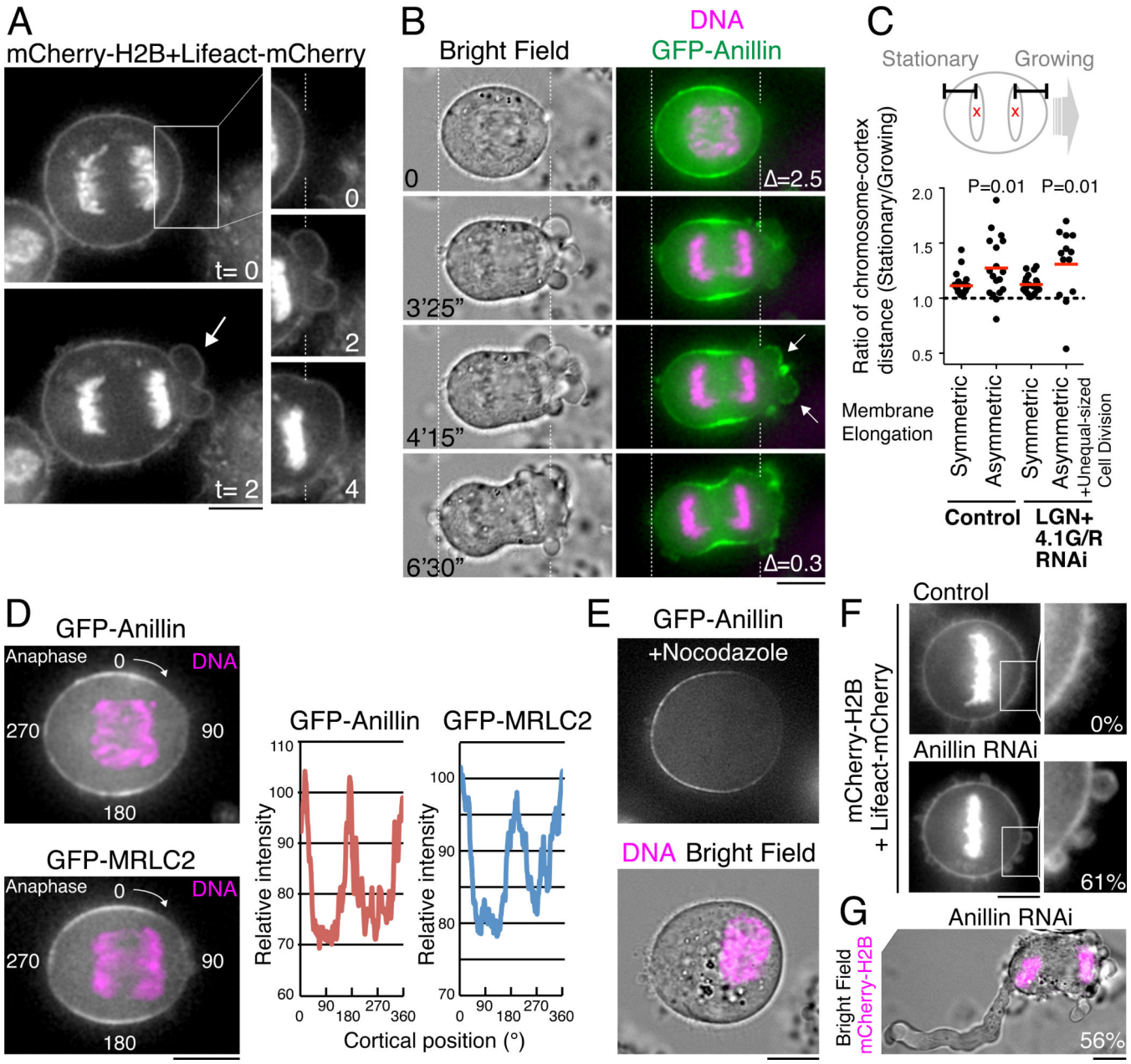

Figure 6. Membrane blebbing drives asymmetric membrane elongation

(*A*) Time-lapse images showing asymmetric membrane blebbing in LGN and 4.1 co-depleted cells. An arrow indicates membrane blebs. (*B*) Time-lapse images of bright field (left), DNA (magenta), and GFP-Anillin (green) in a control cell. Arrows indicate Anillin localization on retracting membrane blebs (Movie S4). (*C*) Scatter plots of the relative ratio of the distance between chromosomes and the stationary or growing cell cortex in symmetrically and asymmetrically elongating control cells (n= 23 and 18, respectively) and LGN and 4.1 co-depleted cells (n= 20 and 13, respectively). Red lines indicate means. P-values indicate statistical significance based on a Student's *t*-test. (*D*) Images of an anaphase cell just prior to asymmetric membrane elongation showing DNA (magenta) and GFP-

Anillin (top) or GFP-MRLC2 (bottom). Right, line scan showing the relative fluorescence intensity of cortical GFP-Anillin and GFP-MRLC2 around the cell cortex. (*E*) Images of a Nocodazole-arrested cell showing GFP-Anillin (top), and bright field and DNA (magenta) (bottom). (*F*) Images of mCherry-H2B and Lifeact-mCherry showing membrane blebbing at metaphase in control (top, n=20) and Anillin depleted (bottom, n=20) cells. Percentages indicate the frequency of blebbing cells in each condition. (*G*) Images showing formation of large membrane blebs in Anillin depleted anaphase cells (56%, n=16). Scale bars, 10 μm. See also Figure S6.

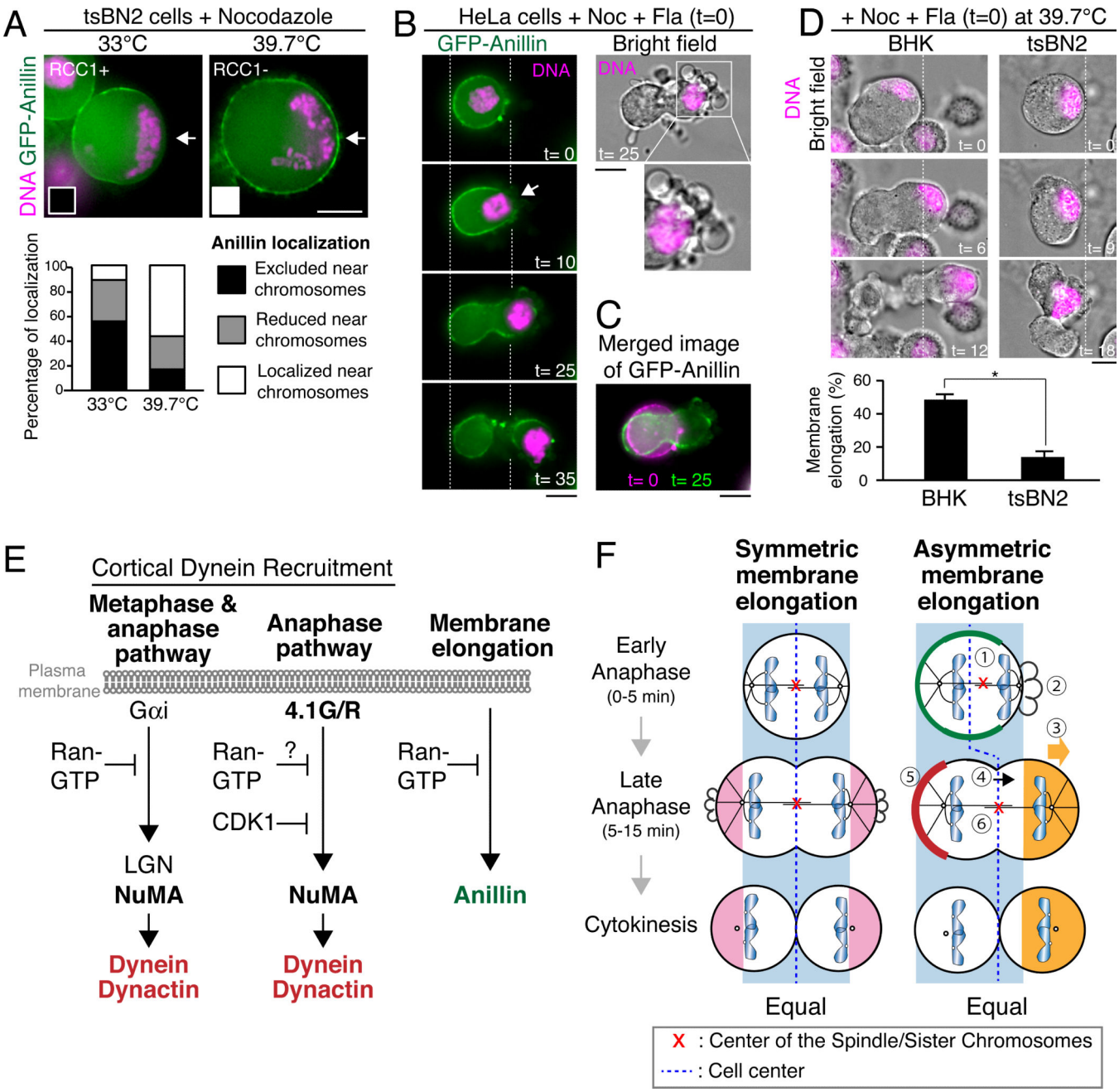

Figure 7. The chromosome-derived Ran-GTP signals locally reduce cortical Anillin to drive membrane elongation

(*A*) Top, fluorescence images of tsBN2 (RCC1^{ts}) cells stably expressing GFP-Anillin. Cells were arrested with nocodazole and then either maintained at the permissive temperature (33°C; n=51) or shifted to the restrictive temperature (39.7°C; n=56). Cells with their chromosomes mass near the cell cortex were observed (arrows). Bottom, histogram showing the quantification of the localization data. (*B*) Time-lapse images of GFP-Anillin (green), DNA (magenta) and bright field in Nodocazole and Flavopiridol treated cells (Movie S8). Cortical GFP-Anillin is locally reduced in the vicinity of the chromosomes (arrow). (*C*) Merged images from (B) at t=0 (magenta) and t=25 min (green). (D) Top, time-lapse images

of Nocodazole- and Flavopiridol-treated BHK (left) and tsBN2 cells at 39.7°C. Dashed lines indicate boundary of cells at t=0. Bottom, graphs showing the frequency of the cells with membrane elongation near the chromosome mass. * indicates statistical difference with 99.9% confidence interval based on a *z*-test. (*E*) Diagram showing pathways for cortical dynein recruitment and membrane elongation. (*F*) Model showing anaphase spindle centering mechanisms. Left, when spindle centering occurs during early anaphase using dynein-dependent forces, cells symmetrically elongate the polar membrane. Right, when the spindle is mis-positioned at the end of early anaphase, the proximity of the chromosomes to the cell cortex [1] induces asymmetric anillin localization (green) [2] to expand the cellular boundary [3]. Although cortical expansion centers the spindle, it also causes cytosolic flow [4] toward the growing cell cortex. Dynein (red) localizes to the stationary cell cortex to anchor the spindle [5] and prevent displacement. These coordinated actions lead to spindle elongation [6] and spindle centering during late anaphase. See also Figure S7.